2020 IEEE/ASME International Conference on
Advanced Intelligent Mechatronics (AIM), Boston, USA
(Virtual Conference), July 6-9, 2020

Kinematic and Kinetic Analysis of 3-RPR Based Robotic Lumbar Brace

Xingzhao Guo, Zhihao Zhou, Jingeng Mai, and Qining Wang, *Senior Member, IEEE*

***Abstract*— Human spine has functions of load-bearing, shock absorption, protection and movement. Spine deformity seriously affects the daily life of patients and reduces the quality of life. Recent ideas of using robotic braces start a new form of rehabilitation for patients with spine deformity. In this paper, we presented a robotic lumbar brace for the potential application to scoliosis rehabilitation. The robotic brace is designed based on a 3-RPR parallel mechanism and consists of three degrees of freedom: horizontal, vertical, and rotational motions of moving platform relative to the fixed platform in the coronal plane. The robotic lumbar brace interferes with the condition of the spine by changing the position of the thorax relative to the pelvis in the coronal plane in order to relieve or correct scoliosis. The linear actuator is customized to meet the need for greater correction force. Kinetic analysis and kinematic analysis which includes inverse kinematics and forward kinematics are demonstrated in detail. The force and moment of robotic lumbar brace support on thorax during the movement can be calculated timely through kinetic analysis. The proposed robotic lumbar brace may have potentials in scoliosis rehabilitation.**

I. Introduction

The spine of human body has functions of load-bearing, shock absorption, protection and movement [1]. Spine deformity seriously affects the daily life of patients and reduces the quality of life, e.g. causing pain, fatigue and numbness [2], [3]. There are usually two treatments for spine deformity: surgical and non-surgical. Surgical treatment may carry an additional risk. Nonsurgical treatment involves brace to correct or relieve spinal deformation [4]–[6]. Current braces in clinical applications can be divided into soft braces and hard ones. However, both kinds of braces are static and cannot be adjusted according to changes in posture in real time. Recent ideas of using robotic braces start a new form of rehabilitation [7].

There are different types of robotic braces. Robotic Spine Exoskeleton (RoSE) [8], [9] consists of two 6 DOFs parallel-actuated modules (Stewart platform) connected in series, each with six actuated limbs. Wheelchair Robot for Active Postural Support (WRAPS) [10] consists of two rings over the hips and chest connected by a 2RPS-2UPS parallel robotic device. WRAPS can modulate the displacement of the upper ring and/or the forces applied on the torso through the ring in four degrees-of-freedom (DOF), including rotations and translation in the sagittal and frontal planes.

In this paper, the proposed robotic brace mainly focuses on rehabilitation of lumbar in coronal plane. Compared with RoSE and WRAPS, although DOF of robotic lumbar brace is reduced, it has higher controllability. In addition, robotic lumbar brace provides greater correcting force. The length of the drive unit is adjustable to change the initial distance between the moving platform and the fixed platform so that robotic lumbar brace can adapt to the subjects with different trunk length. We tried to study the kinematics and kinetics analysis of 3-RPR [11] for robotic lumbar brace in detail. In the inverse kinematics, the manipulator has unique solution. However, in the forward kinematics, the manipulator corresponds to four sets of solutions under the same initial conditions. The workspace of the manipulator is obtained. The teachability of the manipulator can be obtained by the workspace of the manipulator solved, and the unreachable spatial coordinates can be directly filtered out in the control. In order to enable the robotic lumbar brace to provide greater correcting force, we customized the linear actuator with large thrust and small volume without affecting the portability. Through detailed kinematic and dynamic model analysis, controllable ability of 3-RPR parallel manipulator is greatly improved.

The rest of the paper is organized as follows. Section II introduce the mechanism design of the proposed robotic brace. Section III performs kinematic and kinetic analysis. Prototype and simulation results are shown in Section IV. We conclude in Section V.

II. Mechanism design

Robotic lumbar brace consists of moving platform (Thoracic Ring, TR), fixed platform (Pelvic Ring, PR), three linear actuators and other components (Fig. 1). The moving platform and the fixed platform are connected by three linear drive units, and kinematic pair is revolute pair, which constitutes a 3-RPR mechanism. The moving platform of robotic lumbar brace can achieve horizontal, vertical, and rotational motion in the coronal plane.

The manufacturing process of moving platform and fixed platform is shown in Fig. 2. Firstly, 3D scanner (PrimrBot HD6500) was used to scan the subjects' thorax and pelvis, and point cloud on the surface of the thorax and pelvis was obtained. The STL files of the thorax and pelvis 3D model were exported by supporting software corresponding to 3D scanner(Fig. 2(a)). Secondly, it was to edit the model's STL file in the 3D software (PTC Creo 4.0) to obtain the model's surface (Fig. 2(b)). Thirdly, it was to edit the model's

This work was supported by the National Key R&D Program of China (No. 2018YFE0114700), the National Natural Science Foundation of China (No. 51922015, No. 61703007) and the Beijing Natural Science Foundation (No. L182001).

The authors are with the Department of Advanced Manufacturing and Robotics, College of Engineering, Peking University, Beijing 100871, China, with the Beijing Innovation Center for Engineering Science and Advanced Technology (BIC-ESAT), Peking University, China and also with the Beijing Engineering Research Center of Intelligent Rehabilitation Engineering, Beijing 100871, China. (E-mail: qiningwang@pku.edu.cn)

surface of to thorax and pelvis obtain the solid model of the platforms by parametrization modeling(Fig. 2(c)). Finally, the solid model was exported as STL files, which was processed by 3D printing to moving and fix platform (Fig. 2(d)). Considering that the model would be deformed during wearing, Polyamide was used as print material.

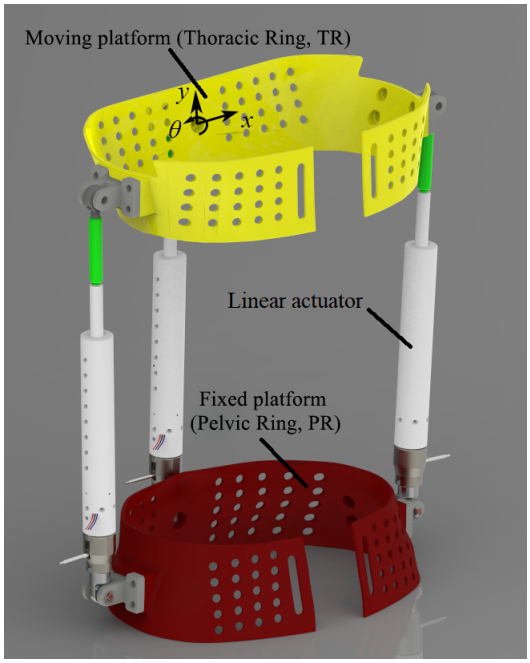

Fig. 1. Robotic Lumbar Spine. Robotic lumbar brace consists of moving platform (TR), fixed platform (PR), three linear actuators and other components.

Table 1 shows detailed parameters in the initial position.

TABLE I
ROBOTIC LUMBAR BRACE PARAMETERS (INITIAL STATE)

	Numerical value
Length	360mm
Width	240mm
Height	450mm
Weight	2.5kg

The drive unit consists of connector of moving platform, extension bar, linear actuator, protecting bush of force sensor, force sensor, connector of fixed platform and other standard parts(Fig. 3). Connector of moving platform is connected with moving platform by a pin shaft, which forms a revolute pair. The function of the extension bar is to adjust the length of the drive unit (Initial state) to suit different subjects because different subjects have different trunk lengths. The linear actuator is the power source of the drive unit, which converts the rotating motion of the motor into the linear output through the screw nut mechanism. The internal angular magnetic encoder module (RMB20IC Incremental with 80 to 2048 pulses per revolution and 320 to 8,192 counts per revolution with x4 evaluation, RLS, Slovenia) is installed to measure the position of the drive unit in real time. Protecting bush of force sensor is designed to protect the force sensor from damaging bending moments. The drive unit is placed in series with load cell (LCM 200 Miniature Tension and Compression Load Cell with IAA100 Analog Amplifier with Voltage Output, FUTEK, USA). Connector of fixed platform is connected with fixed platform by a pin shaft, which forms a revolute pair. Table 2 shows the parameters of the driving unit.

TABLE II
RECOGNITON ACCURACY OF LDA CLASSIFIER

	Numerical value
Nominal voltage	24VDC
Rated current	2.8A
Nominal speed	65mm/s
Torque constant	0.016Nm/A
Screw lead	1mm
Stroke	100mm
Output force	250N
Positional accuracy	1/8400mm
Diameter	24mm
Weight	0.33kg

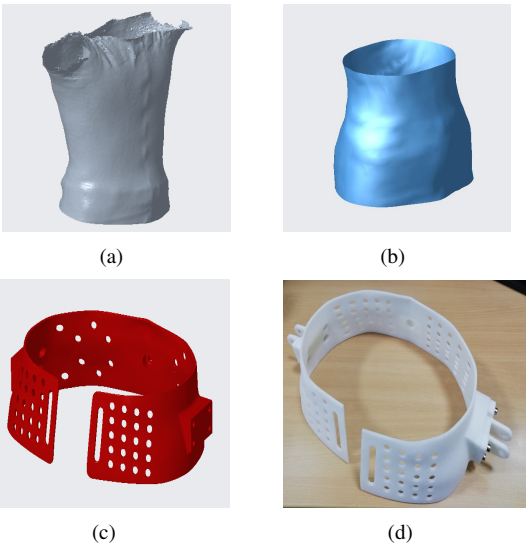

Fig. 2. The manufacturing process of moving platform and fixed platform. (a) The STL files of thorax and pelvis 3D model. (b) Surface of thorax and pelvis model. (c) Solid model of the platforms. (d) 3D printing of moving and fixed platform.

III. KINEMATIC AND KINETIC ANALYSIS

A. Kinematic analysis

Kinematic analysis is to solve the position relationship between the input and output of the manipulator, which is to solve the position of the moving platform in the plane and the rotation Angle relative to the fixed platform. Kinematic analysis includes forward kinematics and inverse kinematics. As we all know, forward kinematics of series manipulator is simple, while the inverse kinematic is complex. Parallel manipulator is the opposite, forward kinematics is complex and inverse kinematics is simple. Therefore, in the process of

kinematic analysis, the inverse kinematic is carried out first, and then the forward kinematic of manipulator is obtained by deducing the inverse kinematic results.

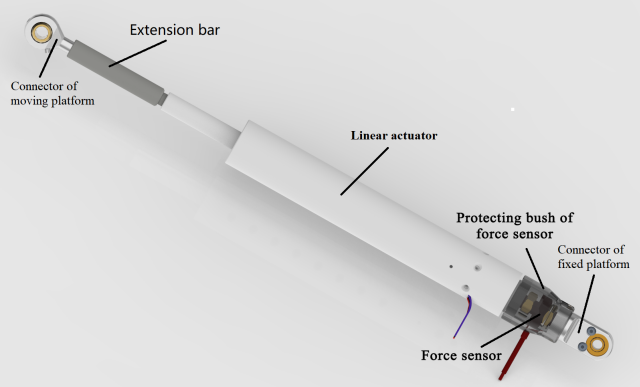

Fig. 3. Assembly of the drive unit. The drive unit includes connector of moving platform, extension bar, linear actuator, protecting bush of force sensor, force sensor, connector of fixed platform and other standard parts.

1) Inverse kinematics: Inverse kinematics analysis is to solve the displacement of the driving element under the condition that the position and posture of moving platform is known. Assuming that the position and posture of moving platform are (x, y, θ) and the displacement of links is (l_1, l_2, l_3). The sketch of mechanism is shown in Fig. 4.

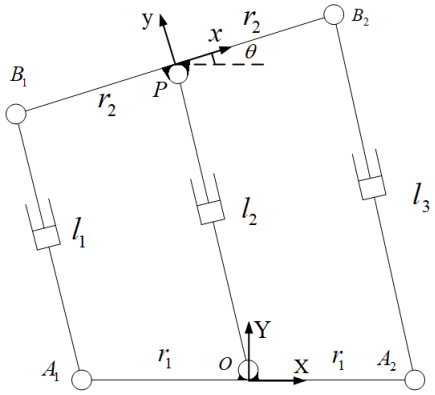

Fig. 4. The 3-RPR sketch. The position and posture of moving platform are $(x, y), \theta$. And the link displacements are (l_1, l_2, l_3).

Referring to Fig. 1,the global coordinate system is set with $X - O - Y$ and the moving coordinate system is set with $x - P - y$. They are represented by $\mathbb{O}$ and $\mathbb{P}$ respectively. Then, coordinates of A_1 and A_2 are $(-r_1, 0)$ and $(r_1, 0)$ respectively in global coordinate system. Coordinates of B_1B_2 are $(-r_2, 0)$ and $(r_2, 0)$ respectively in moving coordinate system. The position and posture of moving platform are expressed with coordinates of P which is (x, y) and θ which is the angle between axis of x and axis of X . The position vector of point B_i in frame $\mathbb{O}$ can be determined using a vector equation $\overrightarrow{OB_i} = \overrightarrow{OP} + \overrightarrow{PB_i}$where $i = 1, 2$. Then, we can get Equation (1).

$$^{\mathbb{O}}\mathbf{r}_{OB_i} = ^{\mathbb{O}}\mathbf{r}_{OP} + ^{\mathbb{O}}\mathbf{R}_{\mathbb{P}}{}^{\mathbb{P}}\mathbf{r}_{PB_i}, i = 1, 2 \tag{1}$$

where(s and c are short for $\sin$ and $\cos$, respectively),
$^{\mathbb{O}}\mathbf{r}_{OB_i} = [B_{iX}, B_{iY}]^T$,
$^{\mathbb{O}}\mathbf{r}_{OP_i} = [x, y]^T$,
$^{\mathbb{O}}\mathbf{R}_{\mathbb{P}} = \begin{bmatrix} c\theta & -s\theta \\ s\theta & c\theta \end{bmatrix}$
Displacement of links can be solved by Equation (2).

$$\begin{cases} l_1 = |\overrightarrow{A_1B_1}| \\ l_2 = |\overrightarrow{OP}| \\ l_3 = |\overrightarrow{A_2B_2}| \end{cases} \tag{2}$$

According to Equation (1) and Equation (2), we can get the equation of links' length, i.e.

$$\begin{cases} l_1 = \sqrt{(x - r_2\cos\theta + r_1)^2 + (y - r_2\sin\theta)^2} \\ l_2 = \sqrt{x^2 + y^2} \\ l_3 = \sqrt{(x + r_2\cos\theta - r_1)^2 + (y + r_2\sin\theta)^2} \end{cases} \tag{3}$$

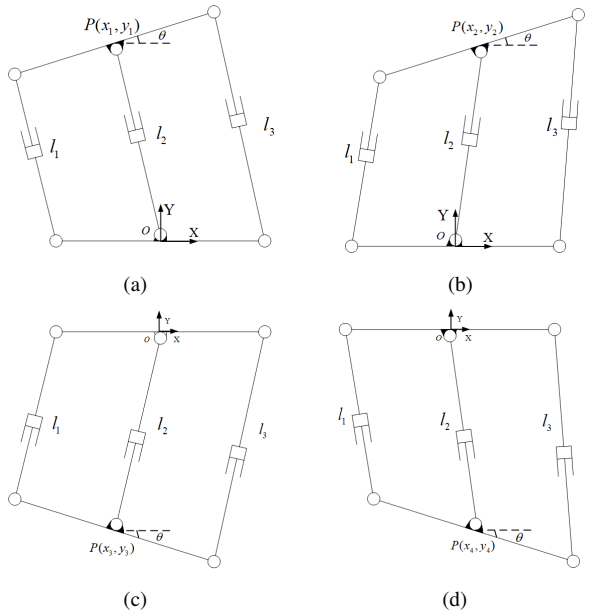

Fig. 5. Four solutions of forward kinematic analysis.

2) Forward Kinematics: Forward kinematic analysis is to solve the position and posture of moving platform under the condition that the displacement of the driving element is known. Let $\cos\theta$ and $\sin\theta$ be replaced with v_1 and v_2, Equation (3) can be rewritten, i.e.

$$\begin{cases} l_1^2 = (x - r_2v_1 + r_1)^2 + (y - r_2v_2)^2 \\ l_2^2 = x^2 + y^2 \\ l_3^2 = (x + r_2v_1 - r_1)^2 + (y + r_2v_2)^2 \\ 1 = v_1^2 + v_2^2 \end{cases} \tag{4}$$

By simplifying Equation (4), we can get the following

equation.

$$\begin{cases} l_3^2 - l_1^2 = 4(r_2v_1 - r_1)x - 4r_2v_2y \\ l_2^2 = x^2 + y^2 \\ l_1^2 + l_3^2 = 2l_2^2 + 2r_2^2 + 2r_1^2 - 4r_1r_2v_1 \\ 1 = v_1^2 + v_2^2 \end{cases} \tag{5}$$

According to Equation (5), v_1 and y can be solved, i.e.

$$v_1 = \frac{2l_2^2 + 2r_2^2 + 2r_1^2 - l_1^2 - l_3^2}{4r_1r_2} \tag{6}$$

$$y = \pm\sqrt{l_2^2 - x^2} \tag{7}$$

It is clear that $\arccos v_1$ has two solutions which are symmetric because of $\theta \in (-\frac{\pi}{2}, \frac{\pi}{2})$.

Considering θ is equal to or greater than 0, the following equation can be acquired according to Equation(5) and Equation (6).

$$l_3^2 - l_1^2 = 4(r_2v_1 - r_1)x + 4r_2v_2\sqrt{l_2^2 - x_2} \tag{8}$$

Equation (8)can be simplified in order to solve for x, i.e.

$$(b^2 + c^2)x^2 - 2abx + a^2 - c^2d^2 = 0 \tag{9}$$

where $a = \frac{l_3^2 - l_1^2}{4}$, $b = r_2v_1 - r_1$, $c = r_2v_2$, and $d = l_2$.

Two solutions can be acquired, i.e.

$$\begin{cases} x_1 = \dfrac{ab + \sqrt{(ab)^2 - (b^2 + c^2)(a^2 - (cd)^2)}}{b^2 + c^2} \\ y_1 = \sqrt{l_2^2 - x_1^2} \\ \theta = \arccos v_1, (\theta \geq 0) \end{cases} \tag{10}$$

$$\begin{cases} x_2 = \dfrac{ab - \sqrt{(ab)^2 - (b^2 + c^2)(a^2 - (cd)^2)}}{b^2 + c^2} \\ y_2 = \sqrt{l_2^2 - x_1^2} \\ \theta = \arccos v_1, (\theta \geq 0) \end{cases} \tag{11}$$

The solutions can be acquired in the same way when θ is less than 0, i.e.

$$\begin{cases} x_3 = \dfrac{ab + \sqrt{(ab)^2 - (b^2 + c^2)(a^2 - (cd)^2)}}{b^2 + c^2} \\ y_3 = -\sqrt{l_2^2 - x_1^2} \\ \theta = \arccos v_1, (\theta < 0) \end{cases} \tag{12}$$

$$\begin{cases} x_4 = \dfrac{ab - \sqrt{(ab)^2 - (b^2 + c^2)(a^2 - (cd)^2)}}{b^2 + c^2} \\ y_4 = -\sqrt{l_2^2 - x_1^2} \\ \theta = \arccos v_1, (\theta < 0) \end{cases} \tag{13}$$

Assume that $l_1 < l_2 < l_3$, four solutions can be acquired according to Equation(10), Equation(11), Equation(12) and Equation(13). Besides, there are no other solutions.Fig.5(a $\sim$ d) correspond to the four solutions.

B. Kinetic analysis

Kinetic analysis is to solve output force and moment of moving platform according to the force of driven unit. Kinetic schematic diagram is shown by Fig. 6. F_1,F_2 and F_3 are thrust of three linear actuators respectively. Assume that the thrust is positive and the pull is negative. Let α and β be angle between X axes and first and third linear actuators respectively.

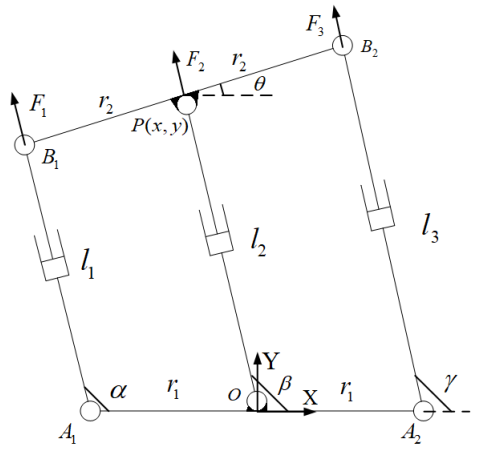

Fig. 6. Kinetic schematic diagram. F_1, F_2 and F_3 are the thrust of three linear actuators respectively. Assume that the thrust is positive and the pull is negative. Let α and β be angle between X axes and first and third linear actuators respectively.

According to forward kinematic analysis, α , β and γ can be solved, i.e.

$$\begin{cases} \cos\alpha = \dfrac{x - r_2\cos\theta + r_1}{(y - r_2\sin\theta)^2 + (x - r_2\cos\theta + r_1)^2} \\ \sin\alpha = \dfrac{y - r_2\sin\theta}{(y - r_2\sin\theta)^2 + (x - r_2\cos\theta + r_1)^2} \end{cases} \tag{14}$$

$$\begin{cases} \cos\beta = \dfrac{x}{y^2 + x^2} \\ \sin\beta = \dfrac{y}{y^2 + x^2} \end{cases} \tag{15}$$

$$\begin{cases} \cos\gamma = \dfrac{x + r_2\cos\theta - r_1}{(y + r_2\sin\theta)^2 + (x + r_2\cos\theta - r_1)^2} \\ \sin\gamma = \dfrac{y + r_2\sin\theta}{(y + r_2\sin\theta)^2 + (x + r_2\cos\theta - r_1)^2} \end{cases} \tag{16}$$

According to orthogonal decomposition of forces, F_1,F_2 and F_3 can be decomposed along X and Y axes, i.e.

$$\begin{cases} F_{1X} = F_1\cos\alpha \\ F_{1Y} = F_1\sin\alpha \end{cases} \tag{17}$$

$$\begin{cases} F_{2X} = F_2\cos\beta \\ F_{2Y} = F_2\sin\beta \end{cases} \tag{18}$$

$$\begin{cases} F_{3X} = F_3\cos\gamma \\ F_{3Y} = F_3\sin\gamma \end{cases} \tag{19}$$

Output force along X and Y axes and moment of moving platform can be solved, i.e.

$$\begin{cases} F_X = F_{1X} + F_{2X} + F_{3X} \\ F_Y = F_{1Y} + F_{2Y} + F_{3Y} \\ M = (F_{1Y} - F_{3Y})r_2 \cos\theta + (F_{3X} - F_{1X})r_2 \sin\theta \end{cases} \tag{20}$$

where M is output moment of moving platform and positive direction of M is counterclockwise.

IV. Results

In the section, wearing effect of robotic lumbar brace is displayed. Besides, the workspace of 3-RPR parallel manipulator is solved [12], [13]. Let $r_1 = 217$ and $r_2 = 195$ according to subject's data.

A. Display of wearing effect

Wearing effect of robotic lumbar brace is shown in Fig. 7. TR and PR are placed in the thorax and pelvis respectively. The low level controllers directly control the motion of the linear actuators. The high level controller is mainly responsible for trajectory planning and zero-torque mode calculation etc. With the cooperation of the high level controller and the low level controller, the moving platform can be controlled to move according to the planed trajectory, which makes thorax have horizontal, vertical, or rotational motion relative to pelvic in the coronal plane.

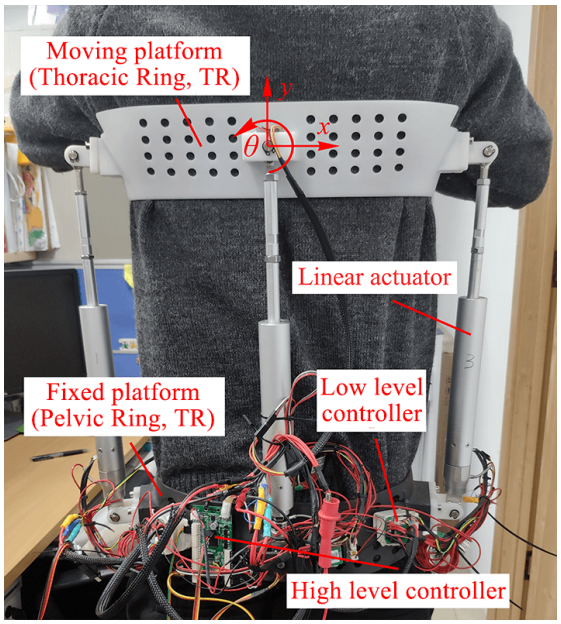

Fig. 7. Wearing effect of Robotic Lumbar Brace. TR and PR are placed in the thorax and pelvis respectively. The low level controllers directly control the motion of the linear actuators. The high level controller is mainly responsible for trajectory planning and zero-torque mode calculation.

B. Global workspace

By simplifying Equation (3), we can get the following equation, i.e.

$$\begin{cases} l_1^2 = (x - r_2\cos\theta + r_1)^2 + (y - r_2\sin\theta)^2 \\ l_2^2 = x^2 + y^2 \\ l_3^2 = (x + r_2\cos\theta - r_1)^2 + (y + r_2\sin\theta)^2 \end{cases} \tag{21}$$

Centroid $P(x, y)$ and the angle θ of moving platform (Fig. 1) will be limited by Equation(21) after range of length of linear actuators is fixed. Range of length of linear actuators is $[340, 440]$, which is decided by specifications of linear actuators.

Centroid $P(x, y)$ of moving platform and length of linear actuators satisfy Equation (21) after θ is constant. Take the maximum and minimum of the length of linear actuators respectively and substitute them into the Equation (21), we can get three regions. Three regions are the circular banded regions with $(r_2\cos\theta - r_1, r_2\sin\theta)$, $(0, 0)$ and $(r_1 - r_2\cos\theta, -r_2\sin\theta)$ as the center of the circle and the maximum and minimum of l_1, l_2 and l_3 as the radius respectively (Fig. 9).

The workspace is then obtained by the intersection of the three foregoing regions. Considering the actual working conditions of robotic lumbar brace, y is greater than 0. Hence, the workspace of manipulator at $0°$ is shown by Fig. 10.

Let the step size of the angle θ is $0.1°$. As for every angle $\theta \in [0, 30]$, we can get a workspace corresponding to it. Then, the workspace of robotic lumbar spine can be obtained by taking the union set of all the obtained workspace corresponding to every angle θ (Fig. 8).

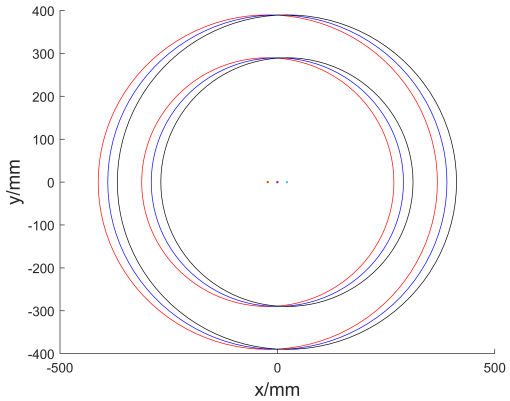

Fig. 9. Three regions are limited by Equation (21) at 0. Three regions are the circular banded regions with $(r_2\cos\theta - r_1; r2\sin\theta)$, (0, 0) and $(r_1 - r_2\cos\theta, -r_2\sin\theta)$ as the center of the circle and the maximum and minimum of l_1, l_2 and l_3 as the radius respectively.

V. Conclusion

In this paper, the structure of the robotic lumbar brace is introduced in detail. The customized linear actuator is introduced and the necessary parameters are given. The kinematics and kinetic analysis of 3-RPR manipulator based

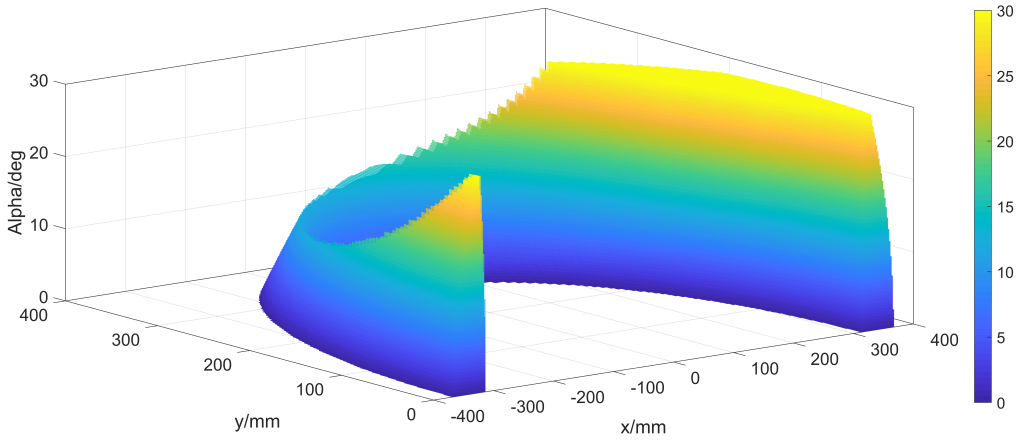

Fig. 8. Rang of motion in the (x, y, θ) obtained for $r_1 = 217, r_2 = 195$ and length of linear actuators $\in [340, 430]$.

on robotic lumbar brace are discussed emphatically. The number and expressions of forward kinematics and inverse kinematics are given. The workspace of the manipulator is obtained. The teachability of the manipulator can be obtained by the workspace of the manipulator solved, and the unreachable spatial coordinates can be directly filtered out in the control. The force and moment of robotic lumbar brace support on thorax during the movement can be calculated timely through kinetic analysis. In the future, the position accuracy in case of no-load and wearing will be verified by more subjects. Besides, we will verify the effect for scoliosis rehabilitation.

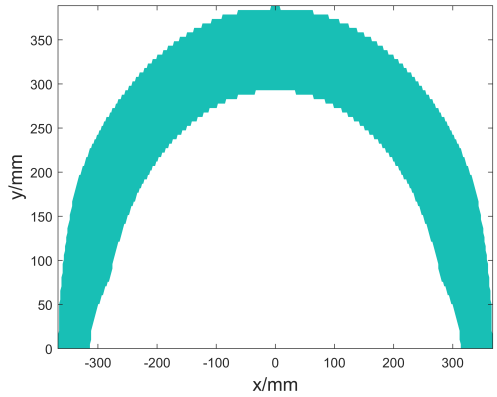

Fig. 10. The workspace at 0. The workspace is then obtained by the intersection of the three foregoing regions.

REFERENCES

[1] I. R. A. Posner, A. A. White, W. T. Edwards, and W. C. Hayes, A biomechanical analysis of the clinical stability of the lumbar and lumbosacral spine, *Spine*, vol. 7, no. 4, pp. 374-389, 1982.

[2] C. Nnadi and J. Fairbank, Scoliosis: A review, *Pediatrics Child Health*, vol. 20, no. 5, pp. 215C220, 2009.

[3] S. L. Weinstein, L. A. Dolan, J. Cheng, A. Danielsson, and J. A. Morcuende, Adolescent idiopathic scoliosis, *The Lancet*, vol. 371, pp.1527-1537, 2008.

[4] R. F. Heary, C. Bono, and S. Kumar, Bracing for scoliosis, *Neurosurgery*, vol. 63, pp. A125CA130, 2008.

[5] S. L. Weinstein, L. A. Dolan, J. G. Wright, and M. B. Dobbs, Effects of bracing in adolescents with idiopathic scoliosis, *New England J. Med.*, vol. 369, no. 16, pp. 1512C1521, 2013.

[6] J. E. Lonstein and R. B. Winter, The milwaukee brace for the treatment of adolescent idiopathic scoliosis: A review of one thousand and twenty patients, *J. Bone Joint Surgery*, vol. 76, no. 8, pp. 1207C1221, 1994.

[7] J. Park, P. Stegall, and S. K. Agrawal, Dynamic brace for correction of abnormal postures of the human spine, *Proc. of the IEEE International Conference on Robotics and Automation*, 2015, pp. 5922-5927.

[8] J. Park, P. R. Stegall, D. P. Roye, and S. K. Agrawal, Robotic Spine Exoskeleton (RoSE): Characterizing the 3-D stiffness of the human torso in the treatment of spine deformity, *IEEE Trans. Neural Systems and Rehabilitation Engineering*, vol. 26, no. 5, pp. 1026-1035, 2018.

[9] R. C. Murray, C. Ophaswongse, J. Park, and S. K. Agrawal, Characterizing torso stiffness in female adolescents with and without scoliosis, *IEEE Robotics and Automation Letters*, vol. 5, no. 2, pp. 1634-1641, 2020.

[10] C. Ophaswongse, R. C. Murray, V. Santamaria, Q. Wang, and S. K. Agrawal, Human evaluation of wheelchair robot for active postural support (WRAPS), *Robotica*, vol. 37, no. 12, pp. 2132-2146, 2019.

[11] X. Kong and C. M. Gosselin, Forward displacement analysis of third-class analytic 3-RPR planar parallel manipulators, *Mechanism and Machine Theory*, vol. 36, pp.1009-1018, 2001.

[12] C. Gosselin and J. Angeles, The optimum kinematic design of a planar three-degree-of-freedom parallel manipulator, *Mechanisms, Transmissions, and Automation in Design*, vol. 110, 1988.

[13] C. M. Gosselin and M. Jean, Determination of the workspace of planar parallel manipulators with joint limits, *Robotics and Autonomous Systems*, vol. 17, pp. 129-138, 1996.